Инфекция и иммунитет
2024, Т. 14, № 5, с. 1002–1016

Russian Journal of Infection and Immunity = Infektsiya i immunitet
2024, vol. 14, no. 5, pp. 1002–1016

BIOSYNTHESIS OF NOVEL MnO_2 NANOCAPSULES VIA *C. SPINOSA* EXTRACT AND HONEYBEE-DERIVED CHITOSAN: EXPLORING ANTIBACTERIAL AND ANTICANCER PROPERTIES

M.G. Elharrif[a], N.A. Hassan[b], M. Sharaf[c,d]

[a] *Shaqra University, Shaqra, Saudi Arabia*
[b] *Chemical Industries Research Institute, National Research Centre, Cairo, Egypt*
[c] *AL-Azhar University, Nasr City, Cairo, Egypt*
[d] *Ocean University of China, Qingdao, PR China*

Abstract. This investigation delves into the integration of *Capparis spinosa* extract (CSLe) onto manganese dioxide nanoparticles (MnO_2NPs) and chitosan derived from honeybees (CSH) in a nanostructured configuration. The resultant nanocomposites, namely CSLe@MnO_2NPs and CSH/CSLe@MnO_2NPs, underwent thorough characterization through various analytical techniques. UV-Vis spectroscopy unveiled distinctive features, such as ligand-to-metal charge transfer and photoluminescence, affirming the successful chitosan-functionalization of the MnO_2NPs, thereby differentiating them from their pristine counterparts. FTIR spectra corroborated the binding of chitosan and identified crucial molecular functional groups. SEM-EDX analysis revealed the morphological properties, addressing non-uniform sizes in the as-calcined MnO_2NPs by the uniform coating of CSH on CSLe@MnO_2NPs, while EDX confirmed the presence of essential elements. TEM and SAED provided insights into the spherical morphology, crystalline structure, and lattice planes of these nanoparticles. Size distribution measurements highlighted distinctions between CSLe@MnO_2NPs and CSH/CSLe@MnO_2NPs. The nanomaterials underwent evaluation for their antimicrobial properties against a spectrum of Gram-negative and Gram-positive bacterial strains, with CSH/CSLe@MnO_2NPs exhibiting the highest bactericidal activity. Additionally, they demonstrated low minimum inhibitory concentration (MIC) values, especially against *S. aureus* (MIC as low as 12.5 μg/ml). Their efficacy extended to anti-biofilm formation, significantly diminishing biofilm development in a dose-dependent manner, a pivotal factor in addressing biofilm-related infections. The study also scrutinized their cytotoxicity against normal Vero and PC3 prostate cancer cells, revealing potential anticancer properties. Dose-dependent reductions in cell viability were observed for both normal and cancer cells. In conclusion, these findings underscore the versatility and promise of CSH/CSLe@MnO_2NPs in diverse biomedical applications, including antibacterial, anti-biofilm, and anticancer therapies.

Key words: *C. spinosa, MnO_2NPs, honeybees chitosan, antibacterial, anti-biofilm, anticancer.*

Адрес для переписки:
Мохаммед Гамаль Эльхарриф
11961, Саудовская Аравия, г. Шакра, факультет фундаментальных медицинских наук, Медицинский колледж, Университет Шакра.
Тел.: +96656364746.
E-mail: al_harrif@yahoo.com

Contacts:
Mohamed Gamal Elharrif
11961, Saudi Arabia, Shaqra, Department of Basic Medical Sciences, College of Medicine, Shaqra University.
Phone: +96656364746.
E-mail: al_harrif@yahoo.com

Для цитирования:
Эльхарриф М.Г. , Хасан Н.А., Шараф М. Биосинтез новых нанокапсул MnO_2 с помощью экстракта c. spinosa и хитозана медоносной пчелы: изучение антибактериальных и противораковых свойств // Инфекция и иммунитет. 2024. Т. 14, № 5. С. 1002–1016. doi: 10.15789/2220-7619-BON-17582

Citation:
Elharrif M.G., Hassan N.A., Sharaf M. Biosynthesis of novel MnO_2 nanocapsules via c. spinosa extract and honeybee-derived chitosan: exploring antibacterial and anticancer properties // Russian Journal of Infection and Immunity = Infektsiya i mmunitet, 2024, vol. 14, no. 5, pp. 1002–1016. doi: 10.15789/2220-7619-BON-17582

DOI: http://dx.doi.org/10.15789/2220-7619-BON-17582

БИОСИНТЕЗ НОВЫХ НАНОКАПСУЛ MnO_2 С ПОМОЩЬЮ ЭКСТРАКТА *C. SPINOSA* И ХИТОЗАНА МЕДОНОСНОЙ ПЧЕЛЫ: ИЗУЧЕНИЕ АНТИБАКТЕРИАЛЬНЫХ И ПРОТИВОРАКОВЫХ СВОЙСТВ

Эльхарриф М.Г.[1], Хасан Н.А.[2], Шараф М.[3,4]

[1] *Университет Шакра, Шакра, Саудовская Аравия*
[2] *Научно-исследовательский институт химической промышленности, Национальный исследовательский центр, Каир, Египет*
[3] *Университет Аль-Азхар, Наср-Сити, Каир, Египет*
[4] *Океанский университет Китая, Циндао, Китай*

Резюме. Настоящее исследование посвящено описанию нанесения экстракта *Capparis spinosa* (CSLE) на наночастицы диоксида марганца (MnO_2NP) и хитозан медоносных пчел (CSH) в наноструктурированной конфигурации. Полученные нанокомпозиты, а именно CSLE@MnO_2NPS и CSH/CSLE@MnO_2NPS, были тщательно охарактеризованы с помощью различных аналитических методов. Спектроскопия в УФ- и видимой области обнаружила отличительные особенности, такие как перенос заряда «лиганд–металл» и фотолюминесценцию, подтверждая успешную функционализацию хитозана на MnO_2NP, тем самым дифференцируя их от соответствующих интактных аналогов. Спектры инфракрасной спектроскопии с преобразованием Фурье (ИКФС) подтвердили связывание хитозана и идентифицировали ключевые молекулярные функциональные группы. Анализ с помощью способа линейного сканирования SEM-EDX выявил морфологические свойства, касающиеся неравномерных размеров кальцинированных MnO_2NP с помощью равномерного покрытия CSH на CSLE@MnO_2NP, в то время как энергодисперсионный рентгеноспектральный микроанализ (EDX) подтвердил наличие необходимых элементов. Просвечивающая электронная микроскопия (TEM) и электронная дифракция на отдельных участках (SAED) дали представление о сферической морфологии, кристаллической структуре и кристаллической плоскости таких наночастиц. Измерения распределения по размерам выявили различия между CSLe@MnO_2NPs и CSH/CSLe@MnO_2NPs. Наноматериалы прошли оценку на антимикробные свойства в отношении различных грамотрицательных и грамположительных бактериальных штаммов, с максимальной бактерицидной активностью у CSH/CSLe@MnO_2NPs. Кроме того, минимальная ингибирующая концентрация (MIC), особенно против *S. aureus* (MIC не более 12,5 мкг/мл) описана при низких значениях. Их эффективность также распространялась на формирование антибиопленки, достоверно дозозависимо снижая образование биопленки как ключевого фактора в отношении инфекций, связанных с биопленкой. Также тщательно изучена цитотоксичность соединений в отношении нормальных клеток Vero и клеток рака предстательной железы PC3, выявившая дозозависимое снижение жизнеспособности клеток обеих линий. Полученные результаты подчеркивают универсальность и перспективность CSH/CSLE@MnO_2NP при использовании в различных биомедицинских целях, включая антибактериальное действие, подавление синтеза антибиопленки и противоопухолевую терапию.

Ключевые слова: *C. spinosa, MnO_2NP, хитозан медоносной пчелы, антибактериальные, антибиопленка, противораковые.*

Introduction

Nanotechnology has significantly transformed the medical landscape, providing innovative solutions to a myriad of healthcare challenges. Manganese dioxide nanoparticles (MnO_2NPs) have garnered substantial attention owing to their unique properties and promising applications in medicine [41]. MnO_2NPs, acting as carriers for therapeutic drugs, facilitate targeted drug delivery to specific cells or tissues, thereby minimizing side effects and amplifying the therapeutic efficacy of medications. The functionalization of MnO_2NPs allows for controlled drug release at the desired location, making them indispensable for personalized medicine and improved treatment outcomes [72].

In the context of healthcare, MnO_2NPs possess diverse pharmacological properties that render them invaluable for medical applications. These properties encompass antioxidant, antimicrobial, neuroprotective, anticancer, and wound-healing attributes. The multifaceted pharmacological profile of MnO_2NPs positions them as promising agents in disease treatment and healthcare, playing a pivotal role in reshaping medical treatments, offering innovative solutions across a spectrum of diseases, and enhancing patient outcomes [57, 66].

Chitosan, a biopolymer derived from chitin found in the shells of crustaceans like shrimp and crabs, is a remarkably versatile material. Particularly intriguing is its utilization when sourced from honeybee exoskeletons in a nanostructured form, a relatively novel and less-explored avenue [2]. Bee-derived chitosan boasts intriguing pharmacological properties with potential applications across various medical and pharmaceutical contexts [33]. It exhibits biocompatibility and biodegradability, making it ideal for drug encapsulation and controlled release, particularly in targeted cancer therapy. Chitosan nanoparticles can target specific tissues or cells, enhanc-

ing drug absorption while minimizing side effects. Additionally, its antimicrobial properties make it effective against bacteria and fungi, useful in wound healing and medical device coatings. Chitosan's ability to form gels and films also supports tissue engineering and regeneration [60].

Capparis spinosa, commonly known as caper, has been utilized in traditional medicine for centuries due to its rich phytochemical composition and diverse pharmacological properties. Key compounds like quercetin, rutin, catechin, and various flavonoids contribute to its therapeutic potential, offering antioxidant, anti-inflammatory, antimicrobial, and potentially anti-diabetic benefits. This botanical extract shows promise in managing conditions such as arthritis, inflammatory bowel diseases, and combating microbial infections, while also potentially regulating blood sugar levels [37].

Incorporating *C. spinosa* into nanostructures presents a promising avenue for enhancing its pharmacological properties. Nanostructured drug delivery systems can significantly improve the bioavailability and therapeutic efficacy of its bioactive compounds. By encapsulating phytochemicals in nanoparticles or nanocarriers, these formulations enhance solubility, enable controlled and sustained release, and target specific cells or tissues, thereby optimizing therapeutic impact while minimizing side effects. This modern approach holds potential for making *C. spinosa* more effective and efficient in various therapeutic applications [3]

Furthermore, nanoencapsulation of *C. spinosa*'s bioactive compounds safeguards them from degradation, boosting stability and shelf life, vital for herbal medicine efficacy. Recent studies have effectively encapsulated these compounds into nanostructures like liposomes and nanoparticles, enhancing pharmacokinetic and pharmacodynamic properties [48]. This advancement in nanomedicine offers promising avenues for improving *C. spinosa*'s therapeutic potential, paving the way for enhanced drug development and natural product-based therapies [34].

Precise targeting of therapies remains a challenge despite the potential of nanostructures for targeted drug delivery. Understanding their interaction with specific cells or tissues is essential. Moreover, comprehensive studies on the long-term effects and potential toxicity of these materials are lacking. Ensuring the biocompatibility and biodegradability of nanostructures is crucial for their safe application in medical treatments. Therefore, the primary goal of this study is to assess the antibacterial and anticancer properties of Manganese Dioxide (MnO_2) combined with extracts from the *C. spinosa* plant, incorporated into nanoparticles and mixed with honeybee-derived chitosan. This innovative combination is being investigated as a potential new pharmacologically active compound. Additionally, we aim to identify and characterize the nanoparticles used in this formulation. This research endeavors to shed light on the potential therapeutic applications of these compounds, addressing both their antimicrobial and anticancer effects

Materials and methods

Plant collection and preparation. C. spinosa, samples were collected from habitats at northwestern coastal region (Alex-Marsa Matrouh Road, 62 km west of El-Hammam city), at the recorded site 30 44 46.88828°N, 29 12 8.0926°E, the collected samples were identified, authenticated taxonomically by the Herbarium, at Desert Research Center, Cairo, Egypt. *C. spinosa*, samples were washed by distilled water then were shade dried at lab-temperature till constant weight. Then, grounded into fine powdery form, sieved and finally stored in dry glass jar at room temperature for further use.

Extraction of natural molecules of C. spinosa, samples. C. spinosa were dried at 60°C till a constant dry weight and ground to powder. Then, 10 g of *C. spinosa*, powder was added to a conical flask with a 100 ml capacity, 5 ml of 2% phenol water, and 10 ml of 30% trichloroacetic acid. After shaking the mixture and letting it sit for a whole night, the filtrate was created up to 50 ml [1].

HPLC. C. spinosa, sample were subjected to identification of phenolic compounds using HPLC. 10 µl of the sample was injection and analyzed at flow rate 0.7 mL/min using Agilent 1200 LC-MS-ESI instrument (positive mode) with a diode array detector set at 254, 280, 320 and 520 nm. Agilent Zorbax Eclipse plus C18 column using nitrogen as nebulizing gas was used. Mobil phase used was 1% formic acid (A) and acetonitrile (B); gradient was 0 min 5% B, 1 min 20% B, 6 min 20% B, 8 min 80% B, 18 min 80% B, 19 min 5% B and 20 min 5%. Mass scanned in the range m/e 0–1000 at fragmentation energy 20 eV and potential 4.0 kV [9].

Chitosan bee's extraction. Several phases were involved in the extraction of biopolymers of chitin and chitosan from a novel potential source which dead corniolan honeybees hybrid were collected in front of bee hives during the autumn season 2022 from the commercial apiary located in Motobes region Kafr El-Sheikh Governorate, Egypt. To extract chitin, the protein (deproteination) and mineral (demineralization) elements of subpestilence are first dissolved and removed. The raw honey bee Apis mellifera material was first ground using (CM 190 Cemotec™, Denmark). Demineralization was then performed using the Hackman technique with minor modifications [21], by treating the crushed raw material with 2 M hydrochloric acid (ratio, 1:10) for 5 h at 25–27°C. Then, deproteination was accomplished by treating the pulverized raw materials with a 1 N sodium hydroxide solution for 1 h at a temperature of 80–85°C. Then, dried at 60–65°C for 4h.

Preparation of CSLe@MnO_2NPs, and CSH/CSLe@MnO_2NPs. Co-precipitation and green chemistry methods were used to synthesize MnO_2NPs. To this end, 0.47 g $KMnO_4$ precursor was dissolved in 20 ml of deionized water. *C. spinosa* extract was then added drop by drop to the previous solution and stirred at 40°C for 2 h using a magnetic stirrer. The resultant solution was dried in an oven at 80°C. The powder obtained was calcined at 400°C for 2 h. For extracted chitosan from dead bees (CHN) solutions was prepared by dissolving 1 g of chitosan in 100 mL of 1.0% aqueous acetic acid and stirring until the liquid became translucent. Then, the CSLE@MnO_2NPs were combined by ionic gelation process with the create bees chitosan. Finally, the suspension was stirred under magnetic stirring at room temperature and left to qualify for 30 min. The bee chitosan NPs were then centrifuged at 3000 rmb for 15 min at 3–5°C and freeze-dried with 10% (m/m) trehalose in a Freeze-dryer for 24 h [5].

Characterization of prepared samples. A PerkinElmer Spectrum 100 Fourier transform infrared (FTIR) spectrometer (PerkinElmer, MA) with an attenuated total reflection (ATR) accessory of germanium crystal with a high-resolution index (4.0), performing 64 scans for each spectrum at 4 cm^{-1} resolution, was used to collect the FTIR spectra of CSLe@MnO_2NPs, and CSH/CSLe@MnO_2NPs samples in the 500–4000 cm^{-1} range [70]. By applying 10 µl of diluted material to holey carbon films on copper grids, TEM was utilized to examine the shape and distribution of the MnO_2NPs, and CSH/CSLe@MnO_2NPs. The samples were seen functioning at a 200 kV accelerating voltage. ImageJ software, version 1.52a, was used to measure nanoparticle size. SEM with EDX analysis (Tescan Vega3, Czechia) was performed at scale levels of 20 µm, 2 µm, 1 µm and 500 nm with the magnification of 1000×, 10,000× and 50,000×. ImageJ software was applied to calculate crystallite size from 2D SEM images. X-ray diffraction (JEOL JDX-3623, Japan) analysis was performed with CuKα (wavelength = 1.5418 Å) radiation from 2θ values of 10° to 80° with applied current and voltage range of 2.5–30 mA and 20–40 kV, respectively [29].

Bacterial sample collection. All the isolated Gram-positive bacteria *Staphylococcus aureus, Staphylococcus hominis*, and *Enterococcus feacalis*, Gram-negative bacteria *Escherichia coli, Klebsiella pneumonia* and *Acinetobacter baumannii* were collected from the Microbiology Department, Faculty of Medicine, Cairo University, Egypt, through the proper protocol and identified and diagnosed based on morphological characteristics and biochemical examinations according to the standard methods of diagnosis and confirmed with the "Vitek 2 compact" [20, 52]

Determination of minimum inhibitory concentration (MICs) and minimum bactericidal concentration (MBCs). By using the usual dilution approach, a broth micro dilution assay was used to estimate the MIC of antibacterial activity in 96 multi-well micro titer plates (CLSI M07-A8). 100 µl of TSB (Himedia) were dispersed evenly across all wells. A volume of 100 µl from each CSLe, CSLe@MnO_2NPs, and CSH/CSLe@MnO_2NPs (1024 — 2.5 µg mL^{-1}) were pipetted into the wells of the first row of the micro titer plate. Finally, 100 µl of freshly made, 0.5 McFarland matching turbid bacterial solution were put to each well. Each plate contained two columns that served as both positive and negative controls. Wrapped plates were incubated for 18–24 h at 37°C. The plates were visually inspected for the presence or absence of turbidity against a dark background. The MIC was determined as the lowest concentration at which there was no discernible bacterial growth when compared to controls. Additionally, stock inoculum suspensions were made in trek diagnostic systems sterile saline with 1% tween 80 from 7 days colonies on potato dextrose agar slants (provided by Remel, Lenexa, Kans) used to estimate the MIC of antifungal activities. A 95% of the stock inoculum suspensions measured 0.9×10^6 to 4.5×10^6 CFU/mL. On test day, each microdilution well was infected with 100 µl of the diluted (Twofold) conidial inoculum suspensions in liquid potato. Then, 200 µl per well of Dextrose Agar (PDA) and microdilution trays were tested after 4 days at 28°C. The MICs goals were the lowest CSLe, CSLe@MnO_2NPs, and CSH/CSLe@MnO_2NPs concentrations that inhibited growth completely (100% inhibition). By sub culturing 20 µl from the clear wells of the MICs and MBCs was ascertained.

Anti-biofilm viability assay. The crystal violet staining test was determined the impact of CSLe, CSLe@MnO_2NPs, and CSH/CSLe@MnO_2NPs on biofilm formation by *S. aureus, S. haemolyticus, E. faecalis, A. baumannii, K. pneumoniae, and E. coli* [19, 62]. In brief, 20 µl of each isolated bacteria was added overnight to growth. Different concentrations of CSLe, CSLe@MnO_2NPs, and CSH/CSLe@MnO_2NPs (1.562 and 25 mg/mL) were added to 180 µL of LB medium with 0.2% (w/v) glucose and incubated at 30°C for 24 h. Then, washing with phosphate buffer pH 7.4 got rid of the planktonic cells, and a 0.1% crystal violet solution was used to color the biofilm that stuck to the surface. After 15 min, sterile-distilled water was used to wash the crystal violet that had been taken apart. Last, the crystal violet that was stuck to the biofilm was released with 200 µl of 95% ethanol. The intensity of the crystal violet at 570 nm was measured with a UV-vis spectrophotometer.

$$\% \text{ Biofilm formation} = (\text{OD control} - \text{OD sample})/(\text{OD control}) \times 100. \quad (1)$$

Evaluation of cytotoxicity by MTT Assay. Both control CSLe, CSLe@MnO_2NPs, and CSH/CSLe@MnO_2NPs conjugates were subjected to cytotoxicity evaluation by MTT assay. For this purpose, Vero

ATCC CCL-81 normal cells and PC3 prostate cancer cell line were used to access the anticancer potential, as reported by [4, 47]. Briefly, Vero ATCC CCL-81 and PC3 cells were grown for 24 h at 37°C in 96-well microtiter plates (pre-inoculated with MnO_2NPs alone, and CSH/CSLe@MnO_2NPs conjugates) using a DMEM that was additionally supplemented with 10% of FBS. After 24 h incubation, the DMEM was removed. The Vero ATCC CCL-81 and PC3 cells were again incubated for 4 h at 37°C in the presence of 20 μL of MTT (5 mg/mL in PBS) supplemented fresh medium. Following that, DMSO (150 μL/well) was used to solubilize the formazan crystals resulting from the mitochondrial reduction of MTT. Finally, the absorbance was recorded at 570 nm (2300 EnSpire Multilabel Plate Reader, Perkin Elmer).

The OD should be directly interrelated to the quantity of cellular activity.

$$\% \text{ Cell viability} = (\text{OD test} - \text{OD blank})/ /(\text{OD control} - \text{OD blank}), \quad (2)$$

where OD optical density, test indicates the cells exposed to the CSLe, CSLe@MnO_2NPs, and CSH/CSLe@MnO_2NPs sample, control in term the control sample, and blank in term the wells without Vero ATCC CCL-81cercopithecus aethiops kidney normal cells and PC3 prostate cancer cell lines.

Statistics analysis. Data was presented as mean± standard error of mean. GraphPad prism software program (version 7.0 (2016) Inc., San Diego, CA, USA) was applied in statistical analysis. The statistical difference among groups was examined by one-way ANOVA subsequently Post hoc-Tukey's test for comparison between groups. All p values (*P < 0.05, **P < 0.01, ***P < 0.001 and ****P < 0.0001), were regarded as statistically significant [44, 45].

Results

HPLC

The HPLC retention durations of the phytoconstituents were compared to the retention periods of the used reference samples to confirm their identities. Four compounds were found in the aqueous extract of the *C. spinosa* after HPLC analysis. Some identification was on the basis of evaluations against current criteria. The substances that were found all products of nature, two compounds of phenolic acids, one compound of each glycoside, and hydroxybenzoate as shown in Fig 1. 19 chemical compounds were identified and purified using HPLC. The percentages of the detected chemicals were computed and compared to the total peaks in the HPLC chromatogram, showing that naringenin (flavonoid), vanillin(organic compound), chlorogenic acid (polyphenol), daidzein (isoflavone), ferulic acid (polyphenol), and methyl gallate (gallate ester) were the major isolated compounds at a concentration of 22.41%, 14.05%, 13.97%, 9.59%, 9.45% and 5.71% respectively. Furthermore the result showed catechin (flavan-3-ol) at a concentration of 2.72%, gallic acid (phenolic acids) at a concentration of 2.89%, coffeic acid (phenolic acids) at a concentration of 3.40%, querectin (flavonol) at a concentration of 0.527%, syringic acid (phenolic acids) at a concentration of 0.250%, rutin (flavonoid) at a concentration of 0.0559%, cinnamic acid (organic compound) at a concentration of 0.0584% and hesperetin (flavonoid) at a concentration of 0.0626%.

Characterization of CSLe@MnO_2NPs, and CSH/CSLe@MnO_2NPs

UV-vis spectroscopic. The UV-visible spectroscopic analysis (Fig. 2A, see cover II) were demonstrated the presence of ligand-to-metal charge transfer from

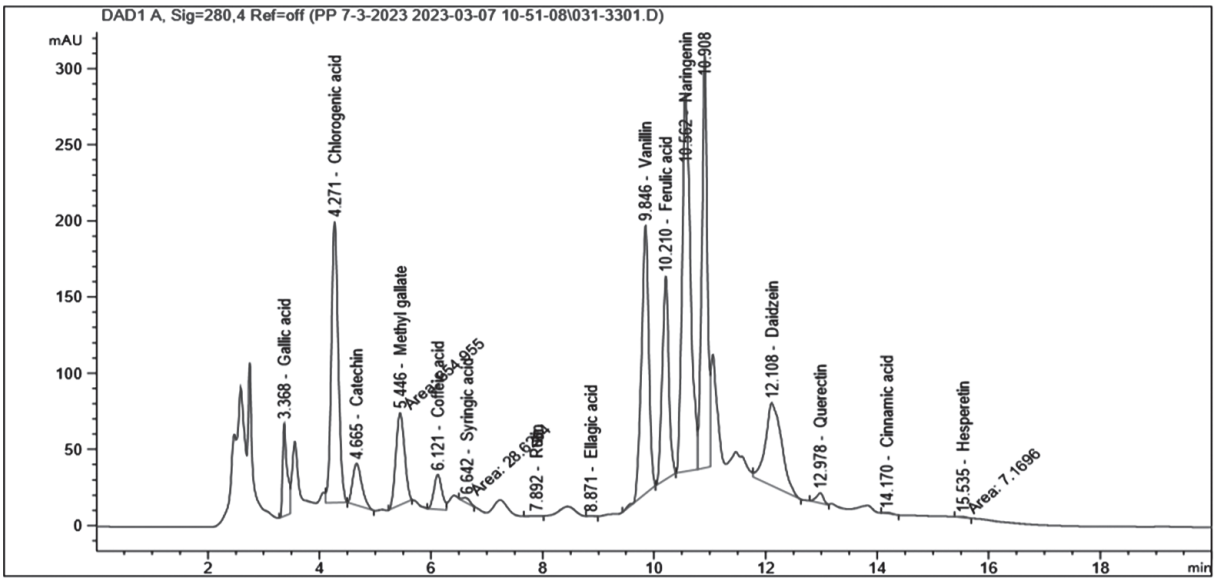

Figure 1. HPLC chromatogram of *C. spinosa* extract

chitosan to Mn^{2+} ions in the MnO_2NPs. Additionally, the room temperature photoluminescence exhibited many distinct characteristics, which are not often seen in unmodified MnO_2NPs. The determination and quantification of the production of chitosan, CSLe@MnO_2NPs, and CSH/CSLe@MnO_2NPs were conducted utilizing the intensity of UV-Vis absorption peaks. Fig. 2A illustrates the presence of a large absorption peak at wavelengths of 350 nm, 245 nm, and 250 nm, respectively.

FTIR spectra. The ligands were generated and the molecules and functional groups were identified by the acquisition of FTIR spectra for the as-calcined MnO_2NPs nanoparticles, CSLe plant, and the composite of MnO_2NPs with Hypericum. The findings are shown in Fig. 2B. The vibrational modes associated with Mn-O-Mn interactions are responsible for the absorption peaks seen within the wavenumber range of 550–650 cm^{-1}. The presence of covalent bonding between the ligand chitosan and the CSLe@MnO_2NPs was verified by the observed alteration in the FTIR spectra, namely in the region associated with the stretching of C-N bonds at a wavenumber of 1210 cm^{-1}. The existence of C-O aromatic carbon compounds is indicated by the absorption peak seen at 1300 cm^{-1} in the combination of CSLe plant and NPs. Furthermore, the presence of CO-O-CO stretching vibrations may be detected by the emergence of a peak at 1050 cm^{-1} and surface OH groups at 3330 cm^{-1} in the CSLe and CSLe@MnO_2NPs, as seen in Fig. 2B.

SEM-EDX. In order to investigate the morphological characteristics of the SCLe@MnO_2NPs, scanning electron microscopy (SEM-EDX) was used. As shown in Fig. 2C, the SEM picture revealed that the SCLe@MnO_2NPs, which were subjected to calcination, exhibited diameters ranging from 22 to 35 nm, as indicated in the inset. The mean size of the NPs is determined to be around 25 nm. It is important to acknowledge that the SCLe@MnO_2NPs exhibit heterogeneity and non-uniformity across various regions as a result of adhesion and agglomeration phenomena. The phenomenon described may be attributed to the process of calcination and subsequent exposure to high temperatures, resulting in the agglomeration of nanoparticles due to their inclination to minimize energy. Fig. 2D displays a scanning electron microscopy (SEM) picture of the composite material consisting of SCLe@MnO_2NPs incorporated with chitosan. The homogenous coating of CSH on the surface of CSLe@MnO_2NPs is evident, indicating the effective attachment of CSH to the composite. This may be attributed to the larger size and less agglomeration of the resultant composite compared to SCLe@MnO_2NPs. In addition, the energy-dispersive X-ray (EDX) spectra of manganese dioxide nanoparticles reveals the presence of oxygen and manganese, with corresponding weight percentages of 40.21% and 60.89%. The provided data illustrates a prominent peak seen at an energy level of 0.2688 kiloelectron volts (keV), which is indicative of the presence of a manganese-oxygen (Mn-O) bond. The presence of elemental peaks of manganese and oxygen in the data supports the conclusion that the production of CSLe@MnO_2NPs has occurred, as seen in Fig. 2E. The composition of the shown elements includes oxygen (11.82%), carbon (21.39%), gold (12.67%), and manganese (54.12%). The findings presented in this study provide confirmation of the successful production of a nanocomposite material consisting of chitosan on CSLe@MnO_2NPs. The low proportion of manganese concentration in the nanocomposite might likely be attributed to the inclusion of manganese dioxide nanoparticles inside the internal porous structure of the chitosan support, as seen in Fig. 2F.

TEM (HRTEM) images and selected area electron diffraction (SAED). In contrast, Fig. 3 illustrates the TEM images of the as-calcined CSLe@MnO_2NPs and composited CSH/CSLe@MnO_2NPs. The TEM images demonstrates that the CSLe@MnO_2NPs have a shape resembling spheres (Fig. 3A). Furthermore, the TEM examination provides further confirmation of the observed accumulation of CSH/CSLe@MnO_2NPs and the subsequent increase in their dimensions (Fig. 3B). The interfering distance of the high-resolution transmission electron microscopy (HRTEM) was measured to be 0.49 nm, indicating the presence of the (101) plane in the crystal lattice of CSLe@MnO_2NPs (refer to Fig. 3C). Additionally, the interfering distance was found to be 0.65 nm, corresponding to the (211) plane of the CSH/CSLe@MnO_2NPs crystal lattice (refer to Fig. 3D).The transmission electron micrographs (TEM) reveal the presence of spherical morphology and uniform dispersion of CSLe@MnO_2 nanoparticles. The electron diffraction pattern obtained from the selected area electron diffraction (SAED) technique exhibits diffraction rings that may be attributed to the (101) and (200) crystallographic planes, as seen in Fig. 3E. The diffraction rings shown in Fig. 3F correspond to the (211) planes, which provide evidence for the presence of the spinel hausmannite structure in the SCH/CSLe@MnO_2NPs. Moreover, the size distribution of NPs were determined and shown in Fig. 3G and H. The experimental findings demonstrated that the CSLe@MnO_2NPs composite exhibited a particle size of 25.27 nm, as shown in Fig. 3G. Additionally, the CSH/CSLe@MnO_2NPs composite displayed a particle size of 98.87 nm, as illustrated in Fig. 3H.

Antimicrobial activity by agar well diffusion assay and MICS and MBC assays

The antibacterial potentialities of pristine CSLe, CSLe@MnO_2NPs, and CSH/CSLe@MnO_2NPs conjugates were evaluated against the bacterial strains of Gram-negative *(A. baumanni, K. pneumoniae* and *E. coli)* and Gram-positive *(S. aureus, S. haemolyticus,* and

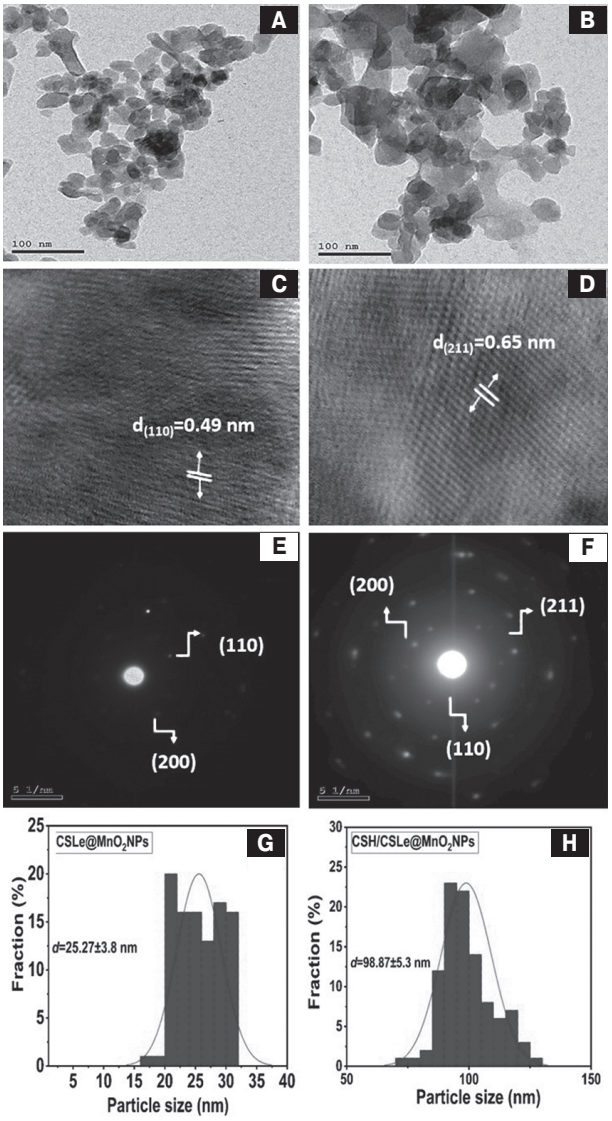

Figure 3. Physico-chemical characterization (A and B) TEM image. (C and D) High-resolution TEM (HRTEM) image and (E and F) SAED pattern of the same. of a single nanoparticle. (G and H) Size distribution measured by TEM of CSLe@MnO_2NPs, and CSH/CSLe@MnO_2NPs composite

E. feacalis) compared to leaves extract of CSLe. The results obtained are listed in Table 1 and shown in Fig. 4 (see cover III). After incubation period, CSLe were found to be bactericidal up to a certain extent against all the tested strains. CSLe were displayed lowest inhibition zone of 21 mm of *E. coli* and the largest inhibition zone of 29 mm of *S. aureus*. However, the experimental results showed that the CSLe@MnO_2NPs are good antibacterial agents. The lowest zones of inhibition have been found as 25 mm for *K. pneumoniae*, and the largest inhibition zone of 31 mm of *S. aureus* and *E. faecalis*. Furthermore, the optimally yielded CSH/CSLe@MnO_2NPs conjugate was found to be highly bactericidal against all test strains. As shown in Fig. 4, zone value reduction from 33 mm against *S. haemolyticus* and 31 mm against *A. baumannii* was recorded.

The broth dilution technique was used to determine the bacteriostatic effects of SCLe, SCLe@MnO_2NPs, and CSH/SCLe@MnO_2NPs against various harmful bacteria. As shown in Table 2, SCLe, and SCLe@MnO_2NPs showed antimicrobial against Gram-negative and Gram-positive bacteria. At low concentrations, However, coated CSH onto SCLe@MnO_2NPs were increased the activity significantly. In contrast, the MIC results revealed that CSH/SCLe@MnO_2NPs were more potent against Gram-negative bacteria than other nanosubstances. The results showed that MIC of the SCLe@MnO_2NPs for the selected Gram-positive bacterial isolates was 12.5 μg/ml of *S. aureus*. While the visual turbidity test showed that CSH/SCLe@MnO_2NPs inhibited *E. coli* and *K. pneumoniae* strains (12.5 μg mL^{-1}) was close to the standard antibiotic gentamicin control inhibition effectiveness varied (8 μg mL^{-1})

Anti-Biofilm Formation

After 24 h treatment and incubation, our findings indicate that the application of SCLe, SCLe@MnO_2NPs, and CSH/SCLe@MnO_2NPs at sub-inhibitory concentrations resulted in a significant decrease in the formation of individual bacterial biofilms, as shown by the observed reduction in OD_{570} nm values. The production of biofilms by *S. aureus, S. haemolyticus, E. faecalis, A. baumannii, K. pneumoniae*, and *E. coli* was shown to decrease in a way that was dependent on the dosage of SCLe, SCLe@MnO_2NPs, and CSH/SCLe@MnO_2NPs, as depicted in Figs. 5A, B, and C. In comparison to the control group, the use of SCLe resulted in a significant decrease in biofilm formation. The greatest inhibitory effect was seen with *S. aureus* bacteria, showing an inhibition rate of around 73.62%. However, the percentage of inhibition was somewhat lower when SCLe was associated with *A. baumanni*, at approximately 73.95% (Fig. 5A). In addition, the experimental investigation involving the application of nano-samples SCLe@MnO_2NPs and CSH/SCLe@MnO_2NPs for the treatment of biofilms revealed noteworthy outcomes. Specifically, the analysis indicated that the bacteria *S. aureus* exhibited the highest inhibition percentage, with rates of approximately 88.89% and 91.16% for SCLe@MnO_2NPs and CSH/SCLe@MnO_2NPs, respectively. Conversely, the bacteria K. pneumoniae demonstrated the lowest inhibition percentage, with rates of about 79.28% and 89.62% for SCLe@MnO_2NPs and CSH/SCLe@MnO_2NPs, respectively (refer to Figs. 5B and C). The quantity of biofilm that developed in the presence of these organisms was contrasted with the quantity of biofilm that formed in their absence. That is, without the use of SCLe, SCLe@MnO_2NPs, and CSH/SCLe@MnO_2NPs. Hence, it can be inferred that the use of chitosan-coated SCLe@MnO_2NPs has promise as a viable therapeutic approach for the management of bacterial infections and perhaps other ailments connected with biofilm formation.

Table 1. Zone diameter (mm) interpretative standards chart and tested samples for the disc diffusion method of determining antimicrobial sensitivity and resistance status of common human bacterial pathogens

No.	Isolate Name	Antibacterial activity (mm)				
		–ve	+ve	SCLe	SCLe @MnO_2NPs	SCH/SCLe@MnO_2NPs
1	*Staphylococcus aureus*	0	25	29	31	34
2	*Staphylococcus haemolyticus*	0	21	23	29	33
3	*Enterococcus faecalis*	0	22	27	31	35
4	*Acinetobacter baumannii*	0	20	22	24	31
5	*Klebsiella pneumoniae*	0	20	22	25	33
6	*Escherichia coli*	0	22	21	26	33

Table 2. MIC determinations of the NPs against fungal and bacterial human pathogens micro-strains

Tested microorganisms	Samples					
	SCLe (mg/ml)		SCLe@MnO_2NPs (μg/ml)		CSH/SCLe@MnO_2NPs (μg/ml)	
	MICs	MBCs	MICs	MBCs	MICs	MBCs
Gram positive bacteria						
E. faecalis	25	100	25	50	50	100
S. aureus	50	100	12.5	25	50	100
S.hominis	50	100	25	50	50	100
Gram negative bacteria						
E. coli	50	100	50	50	12.5	25
K. pneumoniae	50	100	50	50	12.5	25
A. baumannii	25	100	50	50	25	50

Cytotoxicity against and morphological features of normal Vero ATCC CCL-81 and PC3 prostate cancer cells

The literature extensively documents the cytotoxicity of pure metal nanoparticles derived from various sources. Nevertheless, there is a lack of available data regarding the cytotoxicity of MnO_2NPs synthesized using green methods, specifically utilizing leaf extracts from *C. spinosa* and conjugating them with bee chitosan. This cytotoxicity assessment is intended to be conducted on Vero ATCC CCL-81 cells and the PC3 prostate cancer cell line. These nanoparticles have significant potential for various biomedical applications, particularly in combating human carcinoma. To bolster the comprehensiveness of our research, we undertook an inquiry into the cytotoxic properties and anticancer potential of SCLe, SCLe@MnO_2NPs, and CSH/SCLe@MnO_2NPs conjugates. The investigation was conducted on Vero cells, which are considered normal, and PC3 prostate cancer cells. The Vero cells and PC3 cancer cells were cultivated in 96-well microtiter plates at a temperature of 37°C in the presence of each SCLe, SCLe@MnO_2NPs, and CSH/SCLe@MnO_2NPs. Three replicates were performed for each concentration, and an untreated control sample was included in the experiment. The toxicological impact was quantified by evaluating the extent of growth suppression shown by the SCLe, MnO_2NPs, and CSH/SCLe@ MnO_2NPs in relation to the control group, which showed a growth rate of 100%. Fig. 6 (see cover III) illustrates the cytotoxic characteristics of the chemicals under investigation, as represented by the percentage of cellular viability.

The optimally generated CSH/SCLe@MnO_2NPs conjugates showed decreased cell viability in Vero cells and PC3 malignant cells as compared to the control sample. It was shown that this decrease in cell viability was dose-dependent, with a 50% inhibitory concentration (IC_{50}). Furthermore, it was noted that 48 h of incubation were required for the IC50 of the evaluated SCLe, SCLe@MnO_2NPs, and CSH/SCLe@MnO_2NPs conjugates against Vero cells and PC3 cancer cells. The CSH/SCLe@MnO_2 nanoparticle conjugates may have anticancer effects, as shown by the observed inhibitory concentration and rate of cell death/viability. At high doses (250 μg mL^{-1}), a considerable amount of cytotoxicity (83.38%) was detected when Vero cells were exposed to CSH/SCLe@MnO_2NPs. It was found that the IC_{50} values for this therapy were 116.11±3.36 μg mL^{-1}. Comparatively, at the same concentrations, the cytotoxicity of SCLe and MnO_2NPs alone produced lower levels of cytotoxicity (49.68% and 51.54%, respectively). The results showed that the IC_{50} values for SCLe and SCLe@MnO_2NPs alone were 2252.01±4.14 μg mL^{-1} and 245.35±4.9 μg mL^{-1}, in that order (Fig. 6A). Moreover, at high doses of 250 μg/mL^{-1}, PC3 cells treated with CSH/SCLe@MnO_2NPs showed a 69.39% cytotoxic impact. The treatment's IC_{50} values were found to be 205.25±2.53 μg mL^{-1}. By contrast, at the same doses, SCLe and SCLe@MnO_2NPs alone demonstrated cytotoxicity of 55.20% and 64.44%, respectively. The results showed that the IC_{50} values for SCLe and SCLe@MnO_2NPs were 236.84±8.58 μg mL^{-1} and 213.11±3.96 μg mL^{-1}, respectively. Data shown in Fig. 6B.

Morphological features

The morphological properties of PC3 cancer cell lines, untreated normal Vero cell lines, and cell lines treated with different dosages of SCLe, MnO_2NPs, and CSH/SCLe@MnO_2NPs are all reported and compared in this work. The absorbance values acquired from the 3T3 Phototox program were used to determine the amounts of prepared samples in various cell lines. Following the red dye's capture and accounting for the amounts of SCLe, MnO_2NPs, and CSH/SCLe@ MnO_2NPs used in the viability assays, these absorbance values were determined (Figs. 6C and D).

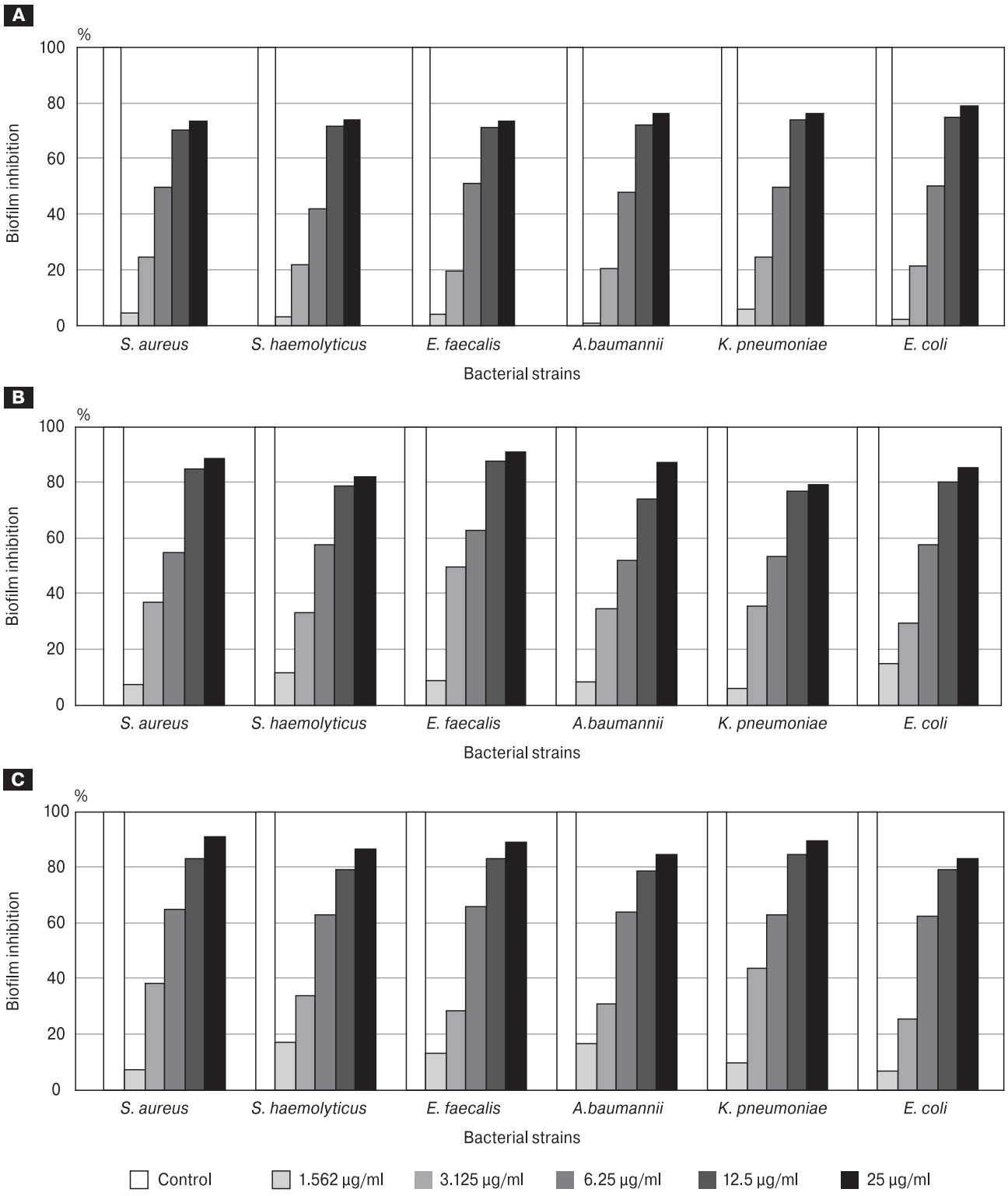

Figure 5. Anti-biofilm activity of (A) SCLe, (B) SCLe@MnO_2NPs, and (C) CSH/SCLe@MnO_2NPs against selected isolated bacteria pathogen's

Discussion

The demand for environmentally friendly synthesis methods for nanoparticles has surged, driven by the widespread use of metal-based nanomaterials in diverse sectors, including industry, medicine, and environmental applications [7]. In recent years, there has been a growing emphasis on harnessing the potential of herbal medicines, abundant in diverse phytometabolites, for the eco-friendly synthesis of nanoparticles. This approach shows promise in combating bacterial infections and contributing to cancer prevention [68]. Consequently, we utilized *C. spinosa* for the synthesis of MnO_2NPs. Through HPLC, we identified and purified 19 chemical compounds. Environmental factors, such as temperature, soil composition, water availability, and humidity, have been shown to impact plant growth, the production of secondary metabolites, and biological activities, potentially reflected in the HPLC results [25]. In our research, we examined the enhanced antibacterial, antibiofilm, and anticancer properties of CSLe when employed in the biofabrication of MnO_2NPs. Importantly, the resulting CSLe@MnO_2NPs did not exhibit cytotoxic effects. Despite using identical source materials, variations in surface composition, aggregation patterns, and nanoparticle sizes gave rise to differences in observed biological activities and NPs related cytotoxicity [46]. The formation of the absorption peak at 350 nm indicated the presence of MnO_2NPs [68]. The intensity of absorption peaks at the same wavelength (350 nm) was used to measure the NPs yield. The peak at 350 nm is due to d–d electron transitions of Mn^{4+} ions in MnO_2NPs [24]. Surface functionalizing ligands, nanoparticle size, and surface charge represent three critical determinants influencing the precise distribution of nanomaterials within living organisms. In this context, we have modified CSLe@MnO_2NPs by introducing a biocompatible ligand, chitosan, owing to its established capacity to selectively target and adhere to the outer membrane of bacteria. This strategic modification is expected to enhance the penetration of MnO_2NPs and their interaction with cellular organelles within microbial cells [25, 46]. According to our findings, FTIR spectra of SCLe, CSLe@ MnO_2NPs and CSH/SCLe@ MnO_2NPs exhibited absorption peaks similar with previous report [67]. Furthermore, TEM and SEM results showed that the particle size of clearly in CSH/SCLe@ MnO_2NPs greater than CSLe@MnO_2NPs which indicates that the addition of CSH increased the size of the SCLe@ MnO_2NPs and the particals size dispersion was in the desired range of reported nano [12, 38]. These observations deviated somewhat from the findings of Fabre et al., 2020 [43], where they observed that unloaded nanoparticles were smaller in size than loaded nanoparticles. The characteristics identified in the EDX analysis align with prior research studies [13, 46, 63].

Our HPLC analysis revealed that the plant extract is rich in phenolic compounds, flavonoids, and terpenoids, known for their active antimicrobial and anti-biofilm properties [56, 69]. Phenolic compounds play a pivotal role in biofilm formation at the cellular level by inducing several significant changes. These changes involve altering the stiffness of the cell wall, increasing the permeability of the cell membrane, and influencing various intracellular processes. These effects occur primarily through the formation of hydrogen bonds between phenolic compounds and enzymes within the cell. This interaction can disrupt the structural integrity of the cell wall, compromise the integrity of the cell membrane, and interfere with essential cellular processes [32]. Consistent with our findings, numerous well-regarded studies have extensively examined the correlation between the antibacterial effectiveness of flavonoids and their structural characteristics. Additionally, several research groups have elucidated the antibacterial mechanisms of specific flavonoids. For instance, the antibacterial activity of quercetin has been attributed to its ability to inhibit DNA gyrase, a critical enzyme involved in bacterial DNA replication and repair processes [11]. Moreover, in a separate study involving different flavonoids tested against various strains of *K. pneumoniae*, all flavonoids demonstrated antimicrobial activity comparable to the standard antibacterial agent ofloxacin. This underscores the potential of flavonoids as effective antimicrobial agents and highlights the diversity of their antibacterial mechanisms [44].

On the other hand, metal oxide nanoparticles, including copper oxide (CuO), manganese oxide (MnO), zinc oxide (ZnO), nickel oxide (NiO), magnesium oxide (MgO), iron oxide (FeO), ferric oxide (Fe_2O_3), and chromium oxide (Cr_2O_3), among others, have garnered significant attention and exploration for various biological applications. These nanoparticles have been extensively studied for their potential in antibacterial, antibiofilm, and anticancer application [55]. Metal oxide nanoparticles exhibit unique properties that make them suitable for a wide range of biological uses. Their antimicrobial properties can help combat bacterial and fungal infections. Our antimicrobial findings align with previous studies by Manjula et al. [41, 50] and Kunkalekar et al. [36], which also observed a stronger inhibitory effect of Manganese dioxide (MnO_2) nanoparticles against Gram-positive bacteria compared to Gram-negative bacteria. This discrepancy in effectiveness might be attributed to diverse mechanisms at play, such as DNA damage and disruption of the bacterial cell membrane. MnO_2NPs have demonstrated a differential impact on Gram-positive and Gram-negative bacteria due to variations in their cell wall structures. The rigid peptidoglycan layer in Gram-positive bacteria makes them more susceptible to damage, including DNA strand breakage, induced by the oxidative stress generated by MnO_2NPs. In contrast, the outer

membrane of Gram-negative bacteria, composed of lipopolysaccharides, provides a protective barrier against some nanoparticles, making them comparatively more resilient [28]. The antibacterial efficacy of CSLe@MnO_2NPs can be attributed to their relatively small size, facilitating their penetration into bacterial cells, and subsequent disruption of the cell membranes. The small size of these nanoparticles allows them to infiltrate the bacterial cells effectively, where they interact with the cell membrane. As a result of this interaction, the cell membrane integrity is compromised, leading to structural damage and permeability changes. These alterations create an environment where vital cellular processes are disrupted, eventually culminating in the demise of the bacterial cell [27]. In a study conducted by Khan et al. [30], they successfully synthesized MnO NPs through the utilization of *A. indicum*, followed by an assessment of the green-synthesized AI-MnONPs. Interestingly, the AI-MnONPs demonstrated a notably high and comparable antibacterial effectiveness against *B. subtilis* and *S. aureus* when compared to conventional antibiotic drugs. This enhanced antibacterial impact could be attributed to a variety of factors, particularly the influence of the nanoparticle structure and composition on key bacterial cell membrane properties [37, 61]. In addition, a study by Souri et al., 2018 [65], manganese oxide nanoparticles were synthesized using lemon extract and curcumin extract. The research yielded compelling results, indicating that MnONPs modified with curcumin and aniline exhibited superior antibacterial effectiveness. These modified MnONPs demonstrated a remarkable capability to prevent the growth of various bacterial pathogens, including *S. aureus, B. subtitles, S. typhi as* well as fungal strains like *C. albicans, C. lunate*, and *T. simii* [22, 58]. In 2015, Azhir and colleagues synthesized manganese trioxide (Mn_3O_4) nanoparticles using the precipitation method. These Mn_3O_4 NPs exhibited robust antimicrobial activity against bacterial pathogens, specifically *E. coli* and *S. aureus*. Notably, when evaluating the antibacterial characteristics of these nanoparticles, a noteworthy observation emerged: *E. coli* displayed a higher degree of sensitivity to Mn_3O_4NPs in comparison to Gram-positive bacteria like *S. aureus*. This discrepancy in response may be attributed to variations in the structural composition of bacterial cell walls [6]. In a separate study, Joshi et al. in 2020 successfully synthesized manganese dioxide nanoparticles, which exhibited notable antimicrobial activity against a range of bacteria, including *S. aureus, P. vulgaris, S. typhi, S. mutants*, and *E. coli* [28]. Likewise, Kumar et al. conducted experiments wherein Mn_3O_4 nanoparticles were prepared at various pH levels, and their antimicrobial properties were assessed using the disk diffusion method. Their findings indicated that these nanoparticles exhibited stronger antibacterial effects against Gram-negative bacteria compared to Gram-positive ones [35]. This differential response is attributed to the presence of negative charge domains on the cell walls of both Gram-positive and Gram-negative bacteria. However, Mn_3O_4 nanoparticles are able to penetrate the outer membrane and interact with the underlying cell wall and membrane components [10]. Our hypothesis revolves around the idea that the increased alkalinity of chitosan-coated SCLe@MnO_2NPs may be attributed to the presence of negatively charged domains on bacterial cell walls. This negative charge is believed to play a significant role in how chitosan-coated SCLe@MnO_2NPs interact with bacterial cell walls, primarily through electrostatic forces or coordination-derived forces. Additionally, it's important to note that metallic nanoparticles often carry a positive charge on their surface, which can further contribute to their ability to disrupt bacterial cell walls and enhance the permeability of nanoparticles into the cells [23, 71].

The broth dilution technique employed to assess the bacteriostatic effects of SCLe, SCLe@MnO_2NPs, and CSH/SCLe@MnO_2NPs against a range of pathogenic bacteria [59]. Notably, the heightened antibacterial effectiveness of CSH/CSLe@MnO_2NPs can be attributed to a synergistic interplay between the physical characteristics of the nanoparticles and the adsorption of bioactive phytomolecules from the leaves extract of *C. spinosa* onto their surface [39]. These results also highlighted that the synthesized CSH/CSLe@MnO_2NPs displayed greater activity against Gram-positive bacteria in contrast to their efficacy against Gram-negative bacterial species. This differential response is likely linked to the structural and compositional differences between the cell walls of Gram-negative and Gram-positive bacterial strains [41]. Nanopolymers, particularly nanochitosan, have been extensively investigated due to their unique bioactivity and their utility as carriers for drug delivery, as well as their antimicrobial, antitumor, and gene delivery capabilities, either in isolation or in combination with other active compounds [15, 18]. Numerous prior studies have also reported similar findings, highlighting the greater efficacy of unmodified chitosan against Gram-negative bacterial strains compared to Gram-positive ones [8, 14, 16, 64].

Numerous research studies have revealed the presence of various anticancer mechanisms linked to chitosan-based nanoparticles. These nanoparticles have exhibited substantial effectiveness in suppressing the proliferation of human carcinoma cell lines in in vitro experiments [26, 51, 53]. In our study, we conducted an evaluation of SCLe, SCLe@MnO_2NPs, and CSH/SCLe@MnO_2NPs in vitro against both normal and cancer cell lines. We aimed to assess their impact on cell morphology and potential cytotoxic effects. To do this, we utilized 3T3 Phototox software to observe identifiable morphological features associated with apoptosis after exposing normal Vero ATCC CCL-81 and PC3 prostate cancer cell lines to these

samples for 24 h. The results of this evaluation revealed concentration-dependent morphological changes in the cells, particularly evident in the concentration range of 250 to 500 μg mL^{-1}. Notably, the enhanced cytotoxicity observed with CSH/SCLe@MnO_2NPs can be linked to an increase in the generation of hydrogen peroxide (H_2O_2). This heightened H_2O_2 production follows the conversion of SCLe crude extract into highly reactive superoxide or hydroxyl radicals [54]. Furthermore, the antioxidant properties and protective effects of the plant extracts can be attributed to the presence of total phenolic, total flavonoid, total saponins, and total alkaloids content in SCLe. These compounds are capable of scavenging free radicals, reducing reactive oxygen species (ROS), and thereby minimizing oxidative stress. Additionally, these phytochemical substances can influence intracellular redox processes and the balance of ROS, leading to the conversion of ROS into highly reactive superoxide or hydroxyl radicals, subsequently resulting in oxidative stress [31, 42]. This oxidative stress can lead to various cellular outcomes, including apoptosis, DNA damage, cytotoxicity, and disruptions in cell signaling [17]. Importantly, after 24 h of incubation with the various cell lines, no discernible cytotoxicity or intracellular ROS generation was observed in any of the samples at doses up to 250 μg mL^{-1}. These findings suggest that chitosan-based nanoparticles may hold significant potential as therapeutic agents for the treatment of human carcinoma. Their selective cytotoxicity towards cancer cells while sparing normal cells makes them promising candidates for further development as anticancer treatments.

Conclusion

In conclusion, this study has successfully developed a straightforward and cost-effective method for synthesizing MnO_2NPs utilizing leaf extracts from *C. spinosa*. The nanoparticles underwent thorough characterization, resulting in the synthesis of CSLe@MnO_2NPs and CSH/CSLe@MnO_2NPs. These nanomaterials exhibited distinctive features, including ligand-to-metal charge transfer and photoluminescence. The introduction of chitosan coating led to more uniform particle sizes. Significantly, these nanomaterials demonstrated potent antibacterial properties against a broad spectrum of bacterial strains, with CSH/CSLe@MnO_2NPs displaying exceptional efficacy. They also exhibited low MIC values, particularly against *S. aureus*. Additionally, the nanomaterials showcased notable anti-biofilm capabilities in a dose-dependent manner, addressing the challenge of biofilm-related infections. Cytotoxicity assessments underscored their potential in anticancer applications, with dose-dependent reductions in cell viability observed in both normal and cancer cells. This comprehensive study highlights the versatility and promise of CSH/CSLe@MnO_2NPs across various biomedical applications, presenting exciting prospects for future research and advancements in the fields of nanomedicine and biotechnology.

Acknowledgements

The author extend their appreciation to the deanship of scientific research at Shaqra University for funding this research work through the project number (SU-ANN-2023059).

Additional information

Ethics approval. The research protocol was reviewed and approved by the ethics committee of the Shaqra University, Saudi Arabia (approval number: ERC_SU_20230033) and all procedures were carried out in accordance with the applicable rules and regulations. The study was carried out in accordance with ARRIVE guidelines.

Competing interests. There are no declared conflicts of interest for the authors.

References

1. Abd-ElGawad A.M., El-Amier Y.A., Assaeed A.M., Al-Rowaily S.L. Interspecific variations in the habitats of Reichardia tingitana (L.) Roth leading to changes in its bioactive constituents and allelopathic activity. *Saudi J. Biol. Sci., 2020, vol. 27, no. 1, pp. 489–499. doi: 10.1016/j.sjbs.2019.11.015*
2. Alqahtani A.S., Nasr F.A., Ahmed M.Z., Bin Mansour M.Y., Biksmawi A.A., Noman O.M., Herqash R.N., Al-zharani M., Qurtam A.A., Rudayni H.A.J.O.C. In vitro protective and anti-inflammatory effects of Capparis spinosa and its flavonoids profile. *Open Chemistry, 2023, vol. 21, no. 1: 20230186. doi: 10.1515/chem-2023-0186*
3. Alshawwa S.Z., Mohammed E.J., Hashim N., Sharaf M., Selim S., Alhuthali H.M., Alzahrani H.A., Mekky A.E., Elharrif M.G. In Situ Biosynthesis of Reduced Alpha Hematite (α-Fe_2O_3) Nanoparticles by Stevia Rebaudiana L. Leaf Extract: Insights into Antioxidant, Antimicrobial, and Anticancer Properties. *Antibiotics (Basel), 2022, vol. 11, no. 9: 1252. doi: 10.3390/antibiotics11091252*
4. Arif M., Sharaf M., Samreen, Khan S., Chi Z., Liu C.G. Chitosan-based nanoparticles as delivery-carrier for promising antimicrobial glycolipid biosurfactant to improve the eradication rate of Helicobacter pylori biofilm. *J. Biomater. Sci. Polym. Ed., 2021, vol. 32, no. 6, pp. 813–832. doi: 10.1080/09205063.2020.1870323*
5. Azhir E., Etefagh R., Mashreghi M., Pordeli P.J.P.C.R. Preparation, characterization and antibacterial activity of manganese oxide nanoparticles. *Physical Chemistry Research, 2015, vol. 3, no. 3, pp. 197–204.*
6. Bakour M., Campos M.d.G., Imtara H., Lyoussi B. Antioxidant content and identification of phenolic/flavonoid compounds in the pollen of fourteen plants using HPLC-DAD. *Journal of Apicultural Research, 2020, vol. 59, no. 1, pp. 35–41.*

7. Bilal M., Zhao Y., Rasheed T., Ahmed I., Hassan S.T.S., Nawaz M.Z., Iqbal H.M.N. Biogenic Nanoparticle–Chitosan Conjugates with Antimicrobial, Antibiofilm, and Anticancer Potentialities: Development and Characterization. *Int. J. Environ. Res. Public Health, 2019, vol. 16, no. 4: 598. doi: 10.3390/ijerph16040598*
8. Ceriello A. Postprandial hyperglycemia and diabetes complications: is it time to treat? *Diabetes, 2005, vol. 54, no. 1, pp. 1–7. doi: 10.2337/diabetes.54.1.1*
9. Chandrasekaran R., Gnanasekar S., Seetharaman P., Keppanan R., Arockiaswamy W., Sivaperumal S. Formulation of Carica papaya latex-functionalized silver nanoparticles for its improved antibacterial and anticancer applications. *J. Mol. Liq., 2016, vol. 219, pp. 232–238.*
10. Cushnie T.P., Lamb A.J. Antimicrobial activity of flavonoids. *Int. J. Antimicrob. Agents, 2005, vol. 26, no. 5, pp. 343–356. doi: 10.1016/j.ijantimicag.2005.09.002*
11. Danaei M., Dehghankhold M., Ataei S., Hasanzadeh Davarani F., Javanmard R., Dokhani A., Khorasani S., Mozafari M.R. Impact of Particle Size and Polydispersity Index on the Clinical Applications of Lipidic Nanocarrier Systems. *Pharmaceutics, 2018, vol. 10, no. 2: 57. doi: 10.3390/pharmaceutics10020057*
12. Dang T.-D., Cheney M.A., Qian S., Joo S.W., Min B.-K. A novel rapid one-step synthesis of manganese oxide nanoparticles at room temperature using poly (dimethylsiloxane). *Ind. Eng. Chem. Res., 2013, vol. 52, no. 7, pp. 2750–2753.*
13. Eaton P., Fernandes J.C., Pereira E., Pintado M.E., Xavier Malcata F. Atomic force microscopy study of the antibacterial effects of chitosans on Escherichia coli and Staphylococcus aureus. *Ultramicroscopy, 2008, vol. 108, no. 10, pp. 1128–1134. doi: 10.1016/j.ultramic.2008.04.015*
14. El Rabey H.A., Almutairi F.M., Alalawy A.I., Al-Duais M.A., Sakran M.I., Zidan N.S., Tayel A.A. Augmented control of drug-resistant Candida spp. via fluconazole loading into fungal chitosan nanoparticles. *Int. J. Biol. Macromol., 2019, vol. 141, pp. 511–516. doi: 10.1016/j.ijbiomac.2019.09.036*
15. Elgadir M.A., Uddin M.S., Ferdosh S., Adam A., Chowdhury A.J.K., Sarker M.Z.I. Impact of chitosan composites and chitosan nanoparticle composites on various drug delivery systems: a review. *J. Food. Drug Anal., 2015, vol. 23, no. 4, pp. 619–629. doi: 10.1016/j.jfda.2014.10.008*
16. Elnosary M.E., Aboelmagd H.A., Habaka M.A., Salem S.R., El-Naggar M.E. Synthesis of bee venom loaded chitosan nanoparticles for anti-MERS-COV and multi-drug resistance bacteria. *Int. J. Biol. Macromol., 2023, vol. 224, pp. 871–880. doi: 10.1016/j.ijbiomac.2022.10.173*
17. Fu P.P., Xia Q., Hwang H.M., Ray P.C., Yu H. Mechanisms of nanotoxicity: generation of reactive oxygen species. *J. Food. Drug Anal., 2014, vol. 22, no. 1, pp. 64–75. doi: 10.1016/j.jfda.2014.01.005*
18. Gan Q., Wang T. Chitosan nanoparticle as protein delivery carrier — systematic examination of fabrication conditions for efficient loading and release. *Colloids Surf. B Biointerfaces, 2007, vol. 59, no. 1, pp. 24–34. doi: 10.1016/j.colsurfb.2007.04.009*
19. Harrigan W.F., McCance M.E. Laboratory methods in food and dairy microbiology. *Academic Press Inc. (London) Ltd., 1976.*
20. Hoseinpour V., Ghaemi N. Novel ZnO–MnO_2–Cu_2O triple nanocomposite: facial synthesis, characterization, antibacterial activity and visible light photocatalytic performance for dyes degradation — a comparative study. *Materials Research Express, 2018, vol. 5, no. 8: 085012.*
21. Ingale A.G., Chaudhari A.N. Biogenic synthesis of nanoparticles and potential applications: an eco-friendly approach. *J. Nanomed. Nanotechol., 2013, vol. 4, no. 165, pp. 1–7. doi: 10.4172/2157-7439.1000165*
22. Jaganyi D., Altaf M., Wekesa I. Synthesis and characterization of whisker-shaped MnO_2 nanostructure at room temperature. *Appl. Nanosci., 2013, vol. 3, pp. 329–333. doi: 10.1007/s13204-012-0135-3*
23. Jayandran M., Muhamed haneefa M., Balasubramanian V. Green synthesis and characterization of Manganese nanoparticles using natural plant extracts and its evaluation of antimicrobial activity. *J. App. Pharm. Sci., 2015, vol. 5, no. 12, pp. 105–110. doi: 10.7324/JAPS.2015.501218*
24. Jeyaraj M., Sathishkumar G., Sivanandhan G., MubarakAli D., Rajesh M., Arun R., Kapildev G., Manickavasagam M., Thajuddin N., Premkumar K., Ganapathi A. Biogenic silver nanoparticles for cancer treatment: an experimental report. *Colloids Surf. B Biointerfaces, 2013, vol. 106, pp. 86–92. doi: 10.1016/j.colsurfb.2013.01.027*
25. Joshi N.C., Joshi E., Singh A. Biological Synthesis, Characterisations and Antimicrobial activities of manganese dioxide (MnO_2) nanoparticles. *Research J. Pharm. and Tech., 2020, vol. 13, no. 1, pp. 135–140.*
26. Joshi N.C., Siddiqui F., Salman M., Singh A. Antibacterial Activity, Characterizations, and Biological Synthesis of Manganese Oxide Nanoparticles using the Extract of Aloe vera. *Asian Pac. J. Health Sci., 2020, vol. 7, no. 3, pp. 27–29. doi: 10.21276/apjhs.2020.7.3.7*
27. Kant R., Pathak S., Dutta V. Design and fabrication of sandwich-structured α-Fe_2O_3/Au/ZnO photoanode for photoelectrochemical water splitting. *Solar Energy Materials and Solar Cells, 2018, vol. 178, pp. 38–45. doi: 10.1016/j.solmat.2018.01.005*
28. Khan S.A., Shahid S., Shahid B., Fatima U., Abbasi S.A. Green Synthesis of MnO Nanoparticles Using Abutilon indicum Leaf Extract for Biological, Photocatalytic, and Adsorption Activities. *Biomolecules, 2020, vol. 10, no. 5: 785. doi: 10.3390/biom10050785*
29. Khanna P., Ong C., Bay B.H., Baeg G.H. Nanotoxicity: an interplay of oxidative stress, inflammation and cell death. *Nanomaterials (Basel), 2015, vol. 5, no. 3, pp. 1163–1180. doi: 10.3390/nano5031163*
30. Khaydarova H.A., Ikhtiyarova G.A., Khaydarova A.A. Method of obtaining a chitosan aminopolisaccharide from behbat Apis Mellifera. *Journal of Chemistry Kazakistan, 2019, no. 2, pp. 69–74.*
31. Khomsi M.E., Imtara H., Kara M., Hmamou A., Assouguem A., Bourkhiss B., Tarayrah M., AlZain M.N., Alzamel N.M., Noman O., Hmouni D. Antimicrobial and Antioxidant Properties of Total Polyphenols of Anchusa italica Retz. *Molecules, 2022, vol. 27, no. 2: 416. doi: 10.3390/molecules27020416*
32. Kravanja G., Primožič M., Knez Ž., Leitgeb M. Chitosan-based (Nano)materials for Novel Biomedical Applications. *Molecules, 2019, vol. 24, no. 10: 1960. doi: 10.3390/molecules24101960*
33. Kulkarni A.P., Srivastava A.A., Nagalgaon R.K., Zunjarrao R.S. Phytofabrication of Silver Nanoparticles from a Novel Plant Source and Its Application. *International Journal of Biological & Pharmaceutical Research, 2012, no. 3, pp. 417–421.*

34. Kumar G.S., Venkataramana B., Reddy S.A., Maseed H., Nagireddy R.R. Hydrothermal synthesis of Mn_3O_4 nanoparticles by evaluation of pH effect on particle Size formation and its antibacterial activity. *Adv. Nat. Sci. Nanosci. Nanotechnol., 2020, no. 11: 035006. doi: 10.1088/2043-6254/ab9cac*
35. Kunkalekar R. Role of oxides (Fe_3O_4, MnO_2) in the antibacterial action of Ag-metal oxide hybrid nanoparticles. *Noble Metal-Metal Oxide Hybrid Nanoparticles. Elsevier, 2019, pp. 303–312.*
36. Li Y., Liu J., Wang L., Zhang J., Wang Z., Gao Z., Zhong Y., Zhang D. Notice of Retraction: Preparation and Characterization of $Mn_{0.5}Zn_{0.5}Fe_2O_4$@Au Composite Nanoparticles and Its Anti-Tumor Effect on Hepatocellular Carcinoma Cells. *5th International Conference on Bioinformatics and Biomedical Engineering. Wuhan, China, 2011, pp. 1–4. doi: 10.1109/icbbe.2011.5781653*
37. Lotfy V.F., Basta A.H. A green approach to the valorization of kraft lignin for the production of nanocomposite gels to control the release of fertilizer. *Biofuels, Bioproducts and Biorefining, 2022, vol. 16, no. 2, pp. 488–498. doi: 10.1002/bbb.2317*
38. Lu H., Zhang X., Khan S.A., Li W., Wan L. Biogenic Synthesis of MnO_2 Nanoparticles With Leaf Extract of Viola betonicifolia for Enhanced Antioxidant, Antimicrobial, Cytotoxic, and Biocompatible Applications. *Front. Microbiol., 2021, no. 12: 761084. doi: 10.3389/fmicb.2021.761084*
39. Majani S.S., Sathyan S., Manoj M.V., Vinod N., Pradeep S., Shivamallu C., Venkatachalaiah K., Kollur S.P. Eco-friendly synthesis of MnO_2 nanoparticles using Saraca asoca leaf extract and evaluation of in vitro anticancer activity. *Current Research in Green and Sustainable Chemistry, 2023, vol. 6: 100367. doi: 10.1016/j.crgsc.2023.100367*
40. Manjula R., Thenmozhi M., Thilagavathi S., Srinivasan R., Kathirvel A. Green synthesis and characterization of manganese oxide nanoparticles from Gardenia resinifera leaves. *Materials Today: Proceedings, 2020, vol. 26, pp. 3559–3563. doi: 10.1016/j.matpr.2019.07.396*
41. Manke A., Wang L., Rojanasakul Y. Mechanisms of nanoparticle-induced oxidative stress and toxicity. *Biomed. Res. Int., 2013, no. 2013: 942916. doi: 10.1155/2013/942916*
42. Marchand G., Fabre G., Maldonado-Carmona N., Villandier N., Leroy-Lhez S. Acetylated lignin nanoparticles as a possible vehicle for photosensitizing molecules. *Nanoscale Adv., 2020, vol. 2, no. 12, pp. 5648–5658. doi: 10.1039/d0na00615g*
43. Mohamed D.I., Alaa El-Din Aly El-Waseef D., Nabih E.S., El-Kharashi O.A., Abd El-Kareem H.F., Abo Nahas H.H., Abdel-Wahab B.A., Helmy Y.A., Alshawwa S.Z., Saied E.M. Acetylsalicylic Acid Suppresses Alcoholism-Induced Cognitive Impairment Associated with Atorvastatin Intake by Targeting Cerebral miRNA155 and NLRP3: In Vivo, and In Silico Study. *Pharmaceutics, 2022, vol. 14, no. 3: 529. doi: 10.3390/pharmaceutics14030529*
44. Mohamed D.I., Ezzat S.F., Elayat W.M., El-Kharashi O.A., El-Kareem H.F.A., Nahas H.H.A., Abdel-Wahab B.A., Alshawwa S.Z., Saleh A., Helmy Y.A., Khairy E., Saied E.M. Hepatoprotective Role of Carvedilol against Ischemic Hepatitis Associated with Acute Heart Failure via Targeting miRNA-17 and Mitochondrial Dynamics-Related Proteins: An In Vivo and In Silico Study. *Pharmaceuticals (Basel), 2022, vol. 15, no. 7: 832. doi: 10.3390/ph15070832*
45. Moon S.A., Salunke B.K., Alkotaini B., Sathiyamoorthi E., Kim B.S. Biological synthesis of manganese dioxide nanoparticles by Kalopanax pictus plant extract. *IET Nanobiotechnol., 2015, vol. 9, no. 4, pp. 220–5. doi: 10.1049/iet-nbt.2014.0051*
46. Morena A.G., Stefanov I., Ivanova K., Perez-Rafael S.l., Sanchez-Soto M., Tzanov T. Antibacterial polyurethane foams with incorporated lignin-capped silver nanoparticles for chronic wound treatment. *Industrial & Engineering Chemistry Research, 2020, vol. 59, no. 10, pp. 4504–4514.*
47. Neamah S.A., Albukhaty S., Falih I.Q., Dewir Y.H., Mahood H.B. Biosynthesis of Zinc Oxide Nanoparticles Using Capparis spinosa L. Fruit Extract: Characterization, Biocompatibility, and Antioxidant Activity. *Appl. Sci., 2023, vol. 13, no. 11: 6604. doi: 10.1016/B978-0-12-822446-5.00010-1*
48. Özçelik B., Orhan D.D., Özgen S., Ergun F. Antimicrobial activity of flavonoids against extended-spectrum β-lactamase (ESβL)-producing Klebsiella pneumoniae. *Tropical Journal of Pharmaceutical Research, 2008, vol. 7, no. 4, pp. 1151–1157. doi: 10.4314/tjpr.v7i4.14701*
49. Pagar T., Ghotekar S., Pagar K., Pansambal S., Oza R. Phytogenic synthesis of manganese dioxide nanoparticles using plant extracts and their biological application. *Handbook of Greener Synthesis of Nanomaterials and Compounds. Elsevier: 2021, pp. 209–218. doi: 10.3390/app13116604*
50. Piao M.J., Kang K.A., Lee I.K., Kim H.S., Kim S., Choi J.Y., Choi J., Hyun J.W. Silver nanoparticles induce oxidative cell damage in human liver cells through inhibition of reduced glutathione and induction of mitochondria-involved apoptosis. *Toxicol. Lett., 2011, vol. 201, no. 1, pp. 92–100. doi: 10.1016/j.toxlet.2010.12.010*
51. Procop G.W., Church D.L., Hall G.S., Janda W.M. Koneman's color atlas and textbook of diagnostic microbiology. *Jones & Bartlett Publishers, 2020. 1830 p.*
52. Qi L.F., Xu Z.R., Li Y., Jiang X., Han X.Y. In vitro effects of chitosan nanoparticles on proliferation of human gastric carcinoma cell line MGC803 cells. *World J. Gastroenterol., 2005, vol. 11, no. 33, pp. 5136–5141. doi: 10.3748/wjg.v11.i33.5136*
53. Raza M.A., Mukhtar F., Danish M. Cuscuta reflexa and Carthamus Oxyacantha: potent sources of alternative and complimentary drug. *Springerplus, 2015, no. 4: 76. doi: 10.1186/s40064-015-0854-5*
54. Razanamahandry L.C., Onwordi C.T., Saban W., Bashir A.K.H., Mekuto L., Malenga E., Manikandan E., Fosso-Kankeu E., Maaza M., Ntwampe S.K.O. Performance of various cyanide degrading bacteria on the biodegradation of free cyanide in water. *J. Hazard Mater., 2019, no. 380: 120900. doi: 10.1016/j.jhazmat.2019.120900*
55. Ríos J.L., Recio M.C. Medicinal plants and antimicrobial activity. *J. Ethnopharmacol., 2005, vol. 100, no. 1–2, pp. 80–84. doi: 10.1016/j.jep.2005.04.025*
56. Sankar Ganesh P., Ravishankar Rai V. Attenuation of quorum-sensing-dependent virulence factors and biofilm formation by medicinal plants against antibiotic resistant Pseudomonas aeruginosa. *J. Tradit. Complement. Med., 2017, vol. 8, no. 1, pp. 170–177. doi: 10.1016/j.jtcme.2017.05.008*
57. Saod W.M., Hamid L.L., Alaallah N.J., Ramizy A. Biosynthesis and antibacterial activity of manganese oxide nanoparticles prepared by green tea extract. *Biotechnol. Rep. (Amst), 2022, vol. 34: e00729. doi: 10.1016/j.btre.2022.e00729*

58. Selim M.S., Fatthallah N.A., Higazy S.A., Chen X., Hao Z. Novel blade-like structure of reduced graphene oxide/α-Mn_2O_3 nanocomposite as an antimicrobial active agent against aerobic and anaerobic bacteria. *Materials Chemistry and Physics, 2023, no. 298: 127436. doi: 10.1016/j.matchemphys.2023.127436*
59. Selim M.S., Hamouda H., Hao Z., Shabana S., Chen X. Design of γ-AlOOH, γ-MnOOH, and α-Mn_2O_3 nanorods as advanced antibacterial active agents. *Dalton Trans., 2020, vol. 49, no. 25, pp. 8601–8613. doi: 10.1039/d0dt01689f*
60. Severino R., Ferrari G., Vu K.D., Donsì F., Salmieri S., Lacroix M. Antimicrobial effects of modified chitosan based coating containing nanoemulsion of essential oils, modified atmosphere packaging and gamma irradiation against Escherichia coli O157: H7 and Salmonella Typhimurium on green beans. *Food Control, 2015, vol. 50, pp. 215–222. doi: 10.1016/j.foodcont.2014.08.029*
61. Shahid S.A., Anwar F., Shahid M., Majeed N., Azam A., Bashir M., Amin M., Mahmood Z., Shakir I. Laser-Assisted synthesis of $Mn_{0.50}Zn_{0.50}Fe_2O_4$ nanomaterial: characterization and in vitro inhibition activity towards bacillus subtilis biofilm. *Journal of Nanomaterials, 2015, vol. 16, no. 1: 111. doi: 10.1155/2015/896185*
62. Sharaf M., Sewid A.H., Hamouda H.I., Elharrif M.G., El-Demerdash A.S., Alharthi A., Hashim N., Hamad A.A., Selim S., Alkhalifah D.H.M., Hozzein W.N., Abdalla M., Saber T. Rhamnolipid-Coated Iron Oxide Nanoparticles as a Novel Multitarget Candidate against Major Foodborne E. coli Serotypes and Methicillin-Resistant S. aureus. *Microbiol. Spectr., 2022, vol. 10, no. 4: e0025022. doi: 10.1128/spectrum.00250-22*
63. Sharma G., Kumar A., Naushad M., García-Peñas A., Al-Muhtaseb A.H., Ghfar A.A., Sharma V., Ahamad T., Stadler F.J. Fabrication and characterization of Gum arabic-cl-poly(acrylamide) nanohydrogel for effective adsorption of crystal violet dye. *Carbohydr. Polym., 2018, vol. 202, pp. 444–453. doi: 10.1016/j.carbpol.2018.09.004*
64. Silva L.P. da, de Britto D., Seleghim M.H.R., Assis O.B.G. In vitro activity of water-soluble quaternary chitosan chloride salt against E. coli. *World Journal of Microbiology and Biotechnology, 2010, vol. 26, no. 11, pp. 2089–2092.*
65. Souri M., Hoseinpour V., Shakeri A., Ghaemi N. Optimisation of green synthesis of MnO nanoparticles via utilising response surface methodology. *IET Nanobiotechnol., 2018, vol. 12, no. 6, pp. 822–827. doi: 10.1049/iet-nbt.2017.0145*
66. Srinivasa C., Kumar S.R.S., Pradeep S., Prasad S.K., Veerapur R., Ansari M.A., Alomary M.N., Alghamdi S., Almehmadi M., Gc K., Daphedar A.B., Kakkalameli S.B., Shivamallu C., Kollur S.P. Eco-Friendly Synthesis of MnO_2 Nanorods Using Gmelina arborea Fruit Extract and Its Anticancer Potency Against MCF-7 Breast Cancer Cell Line. *Int. J. Nanomedicine, 2022, vol. 17, pp. 901–907. doi: 10.2147/IJN.S335848*
67. Sun S.-N., Li M.-F., Yuan T.-Q., Xu F., Sun R.-C. Effect of ionic liquid/organic solvent pretreatment on the enzymatic hydrolysis of corncob for bioethanol production. Part 1: Structural characterization of the lignins. *Industrial Crops and Products, 2013, vol. 43, pp. 570–577. doi: 10.1016/j.indcrop.2012.07.074*
68. Suzuki S., Miyayama M. Structural Distortion in MnO_2 Nanosheets and Its Suppression by Cobalt Substitution. *Nanomaterials (Basel), 2017, vol. 7, no. 10: 295. doi: 10.3390/nano7100295*
69. Svirska S., Grytsyk A.Investigation of tannins in Anchusa officinalis L. *Pharma Innovation, 2018, vol. 7, no. 4, pp. 758–761.*
70. Taleb F., Ammar M., Mosbah M.B., Salem R.B., Moussaoui Y. Chemical modification of lignin derived from spent coffee grounds for methylene blue adsorption. *Sci. Rep., 2020, vol. 10, no. 1: 11048. doi: 10.1038/s41598-020-68047-6*
71. Vashistha V.K., Gautam S., Bala R., Kumar A., Das D.K. Transition Metal-Based Nanoparticles as Potential Antimicrobial Agents. *Reviews and Advances in Chemistry, 2022, vol. 12, no. 4, pp. 222–247.*
72. Xia H.-Y., Li B.-Y., Zhao Y., Han Y.-H., Wang S.-B., Chen A.-Z., Kankala R.K. Nanoarchitectured manganese dioxide (MnO_2)-based assemblies for biomedicine. *Coordination Chemistry Reviews, 2022, vol. 464: 214540. doi: 10.1016/j.ccr.2022.214540*
73. Zhang H., Ma Z.F. Phytochemical and Pharmacological Properties of Capparis spinosa as a Medicinal Plant. *Nutrients, 2018, vol. 10, no. 2: 116. doi: 10.3390/nu10020116*

Авторы:

Эльхарриф М.Г., PhD, кафедра фундаментальных медицинских наук, Медицинский колледж, Университет Шакра, Шакра, Саудовская Аравия;
Хасан Н.А., PhD, отдел синтеза, кафедра фотохимии, Научно-исследовательский институт химической промышленности, Национальный исследовательский центр, Каир, Египет;
Шараф М., PhD, кафедра биохимии и молекулярной биологии, колледж наук о морской жизни, Океанский университет Китая, Циндао, Китай.

Authors:

Elharrif M.G., PhD, Department of Basic Medical Sciences, College of Medicine, Shaqra University, Shaqra, Saudi Arabia;
Hassan N.A., PhD, Synthetic Unit, Department of Photochemistry, Chemical Industries Research Institute, National Research Centre, Cairo, Egypt;
Sharaf M., PhD, Department of Biochemistry and Molecular Biology, College of Marine Life Sciences, Ocean University of China, Qingdao, China.

Поступила в редакцию 29.01.2024
Отправлена на доработку 08.03.2024
Принята к печати 06.04.2024

Received 29.01.2024
Revision received 08.03.2024
Accepted 06.04.2024

Иллюстрации к статье «Биосинтез новых нанокапсул MnO_2 с помощью экстракта *C. spinosa* и хитозана медоносной пчелы: изучение антибактериальных и противораковых свойств» (авторы: М.Г. Эльхарриф, Н.А. Хасан, М. Шараф) (с. 1002–1016)

Illustrations for the article "Biosynthesis of novel MnO_2 nanocapsules via *C. spinosa* extract and honeybee-derived chitosan: exploring antibacterial and anticancer properties" (authors: Elharrif M.G., Hassan N.A., Sharaf M.) (pp. 1002–1016)

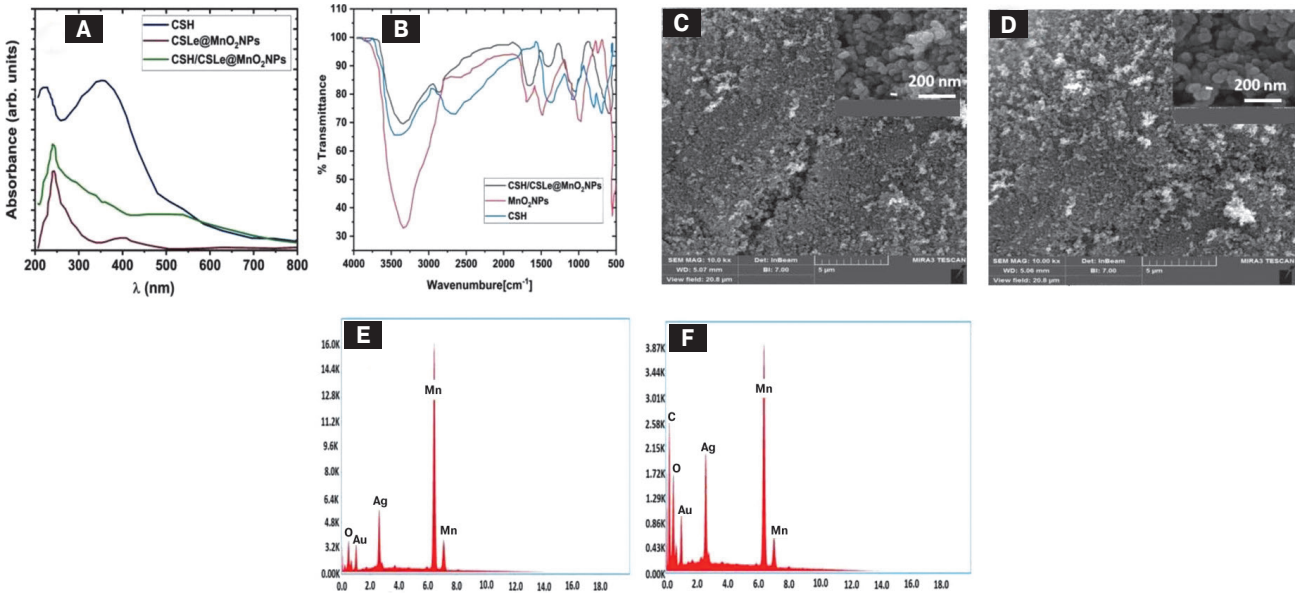

Figure 2. Physico-chemical characterization (A) UV-Vis spectroscopic, (B) FTIR of CSH, CSLe@MnO_2NPs, and CSH/CSLe@MnO_2NPs, (C and D) SEM image (magnification 5 μm and 200 nm), and (E and F) EDX microphotographs of CSLe@MnO_2NPs, and CSH/CSLe@MnO_2NPs composite

Иллюстрации к статье «Биосинтез новых нанокапсул MnO_2 с помощью экстракта *C. spinosa* и хитозана медоносной пчелы: изучение антибактериальных и противораковых свойств» (авторы: М.Г. Эльхарриф, Н.А. Хасан, М. Шараф) (с. 1002–1016)

Illustrations for the article "Biosynthesis of novel MnO_2 nanocapsules via *C. spinosa* extract and honeybee-derived chitosan: exploring antibacterial and anticancer properties" (authors: Elharrif M.G., Hassan N.A., Sharaf M.) (pp. 1002–1016)

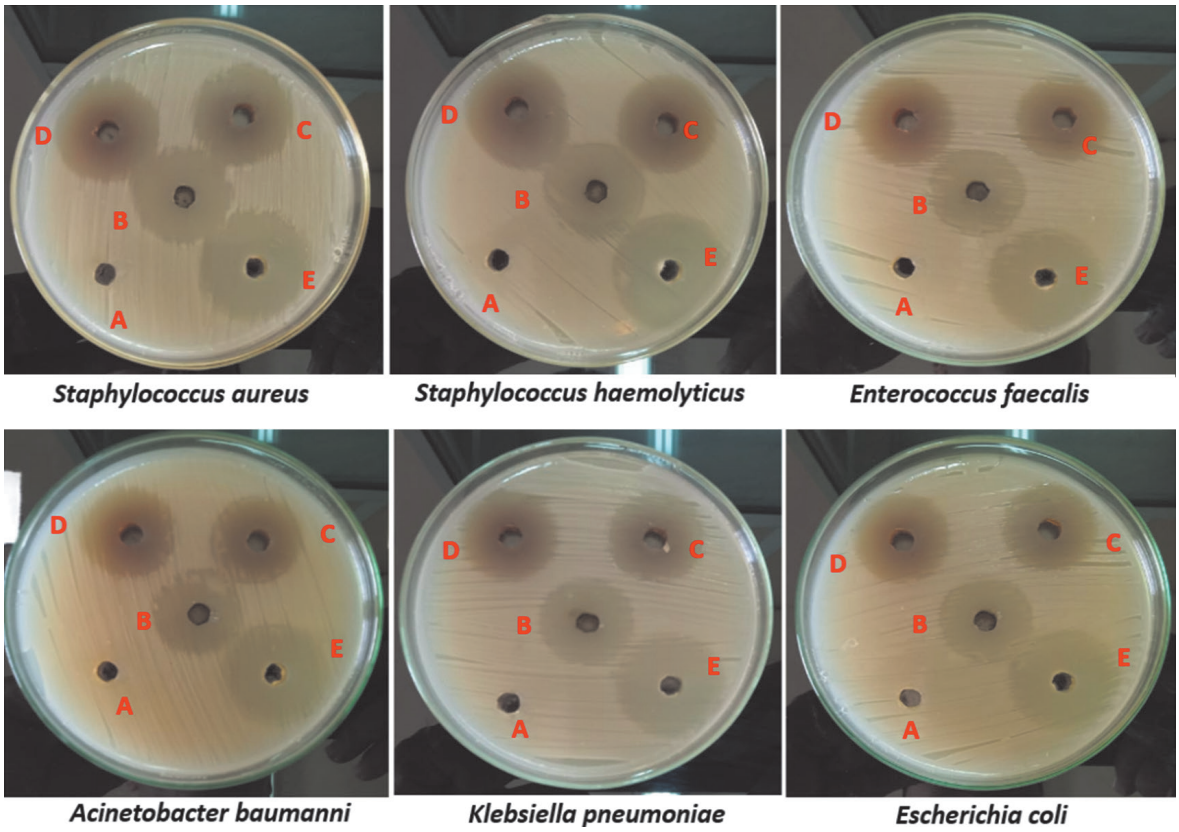

Figure 4. The inhibition zone of different pathogenic bacteria strains *S. aureus, S. hominis, E. faecalis, A. baumannii, K. pneumoniae,* and *E. coli* against by (A) negative control (dH_2O), (B) positive control, (C) SCLe, (D) SCLe@MnO_2NPs, and (E) CSH/SCLe@MnO_2NPs

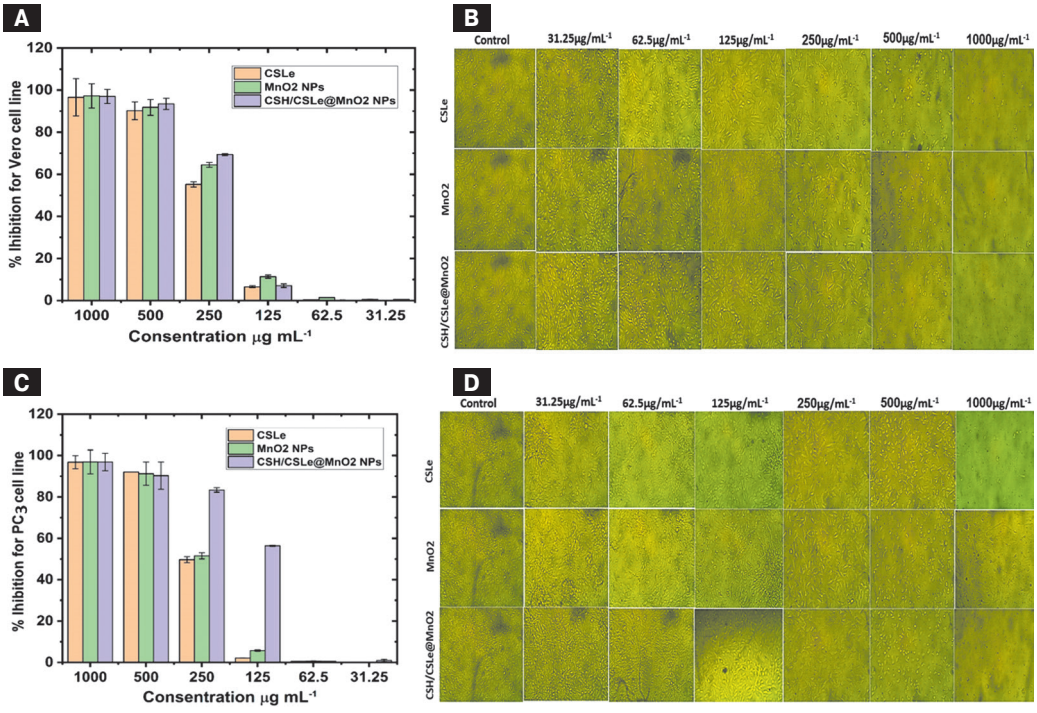

Figure 6. Cytotoxicity of SCLe, MnO_2NPs, and CSH/SCLe@MnO_2NPs on normal Vero cells (A and B), and prostate carcinoma PC3 cells (C and D) for 24 h. The results were taken from replicated (n = 3) (Mean±SD). (B and D) Morphological features, the images were taken from the cells were treated with an average size of 10 nm for 24 h